Manipulating coherence resonance in a quantum dot semiconductor laser via electrical pumping

Christian Otto,[1,2] Benjamin Lingnau,[1] Eckehard Schöll,[1] and Kathy Lüdge[1,*]

[1] *Institut für Theoretische Physik, Technische Universität Berlin, Hardenbergstr. 36, 10623 Berlin, Germany*

[2] *Potsdam Institute for Climate Impact Research, Telegraphenberg A 31, 14473 Potsdam, Germany*

[*] *luedge@physik.tu-berlin.de*

Abstract: Excitability and coherence resonance are studied in a semiconductor quantum dot laser under short optical self-feedback. For low pump levels, these are observed close to a homoclinic bifurcation, which is in correspondence with earlier observations in quantum well lasers. However, for high pump levels, we find excitability close to a boundary crisis of a chaotic attractor. We demonstrate that in contrast to the homoclinic bifurcation the crisis and thus the excitable regime is highly sensitive to the pump current. The excitability threshold increases with the pump current, which permits to adjust the sensitivity of the excitable unit to noise as well as to shift the optimal noise strength, at which maximum coherence is observed. The shift adds up to more than one order of magnitude, which strongly facilitates experimental realizations.

© 2014 Optical Society of America

OCIS codes: (140.5960) Semiconductor lasers; (190.1450) Bistability; (230.5590) Quantum-well, -wire and -dot devices.

References

1. D. Bimberg, M. Grundmann, and N. N. Ledentsov, *Quantum Dot Heterostructures* (John Wiley & Sons Ltd., New York, 1999).
2. K. Lüdge, *Nonlinear Laser Dynamics-From Quantum Dots to Cryptography* (Wiley-VCH, 2012).
3. M. Gioannini, and I. Montrosset, "Numerical analysis of the frequency chirp in quantum-dot semiconductor lasers," IEEE J. Quantum Electron. **43**, 941–949 (2007).
4. B. Lingnau, K. Lüdge, W. W. Chow, and E. Schöll, "Failure of the α-factor in describing dynamical instabilities and chaos in quantum-dot lasers," Phys. Rev. E **86**, 065201(R) (2012).
5. B. Lingnau, W. W. Chow, E. Schöll, and K. Lüdge, "Feedback and injection locking instabilities in quantum-dot lasers: a microscopically based bifurcation analysis," New J. Phys. **15**, 093031 (2013).
6. T. Erneux, E. A. Viktorov, and P. Mandel, "Time scales and relaxation dynamics in quantum-dot lasers," Phys. Rev. A **76**, 023819 (2007).
7. K. Lüdge, E. Schöll, E. A. Viktorov, and T. Erneux, "Analytic approach to modulation properties of quantum dot lasers," J. Appl. Phys. **109**, 103112 (2011).
8. J. Pausch, C. Otto, E. Tylaite, N. Majer, E. Schöll, and K. Lüdge, "Optically injected quantum dot lasers - impact of nonlinear carrier lifetimes on frequency locking dynamics," New J. Phys. **14**, 053018 (2012).
9. C. Otto, K. Lüdge, E. A. Viktorov, and T. Erneux, "Quantum dot laser tolerance to optical feedback," in "Nonlinear Laser Dynamics - From Quantum Dots to Cryptography," , K. Lüdge, ed. (WILEY-VCH, Weinheim, 2012), Chap. 6, pp. 141–162.
10. S. Wilkinson, B. Lingnau, J. Korn, E. Schöll, and K. Lüdge, "Influence of noise on the signal properties of quantum-dot semiconductor optical amplifiers," IEEE J. Sel. Top. Quantum Electron. **19**, 1900106 (2013).

#206726 - $15.00 USD Received 20 Feb 2014; revised 11 Apr 2014; accepted 6 May 2014; published 27 May 2014
(C) 2014 OSA

11. S. Perrone, R. Vilaseca, and C. Masoller, "Stochastic logic gate that exploits noise and polarization bistability in an optically injected vcsel," Opt. Express **20**, 22692–22699 (2012).
12. V. Flunkert, O. D'Huys, J. Danckaert, I. Fischer, and E. Schöll, "Bubbling in delay-coupled lasers," Phys. Rev. E **79**, 065201 (R) (2009).
13. M. C. Soriano, J. García-Ojalvo, C. R. Mirasso, and I. Fischer, "Complex photonics: Dynamics and applications of delay-coupled semiconductors lasers," Rev. Mod. Phys. **85**, 421–470 (2013).
14. A. L. Hodgkin, "The local electric changes associated with repetitive action in a medullated axon," J. Physiol. **107**, 165 (1948).
15. J. D. Murray, *Mathematical Biology*, 2nd ed. of Biomathematics Texts (Springer, Berlin Heidelberg, 1993), vol. 19.
16. A. N. Zaikin, and A. M. Zhabotinsky, "Concentration wave propagation in two-dimensional liquid-phase self-oscillating system," Nature **225**, 535–537 (1970). 10.1038/225535b0.
17. D. Goulding, S. P. Hegarty, O. Rasskazov, S. Melnik, M. Hartnett, G. Greene, J. G. McInerney, D. Rachinskii, and G. Huyet, "Excitability in a quantum dot semiconductor laser with optical injection," Phys. Rev. Lett. **98**, 153903 (2007).
18. B. Kelleher, D. Goulding, S. P. Hegarty, G. Huyet, D. Y. Cong, A. Martinez, A. Lemaitre, A. Ramdane, M. Fischer, F. Gerschütz, and J. Koeth, "Excitable phase slips in an injection-locked single-mode quantum-dot laser," Opt. Lett. **34**, 440–442 (2009).
19. B. Kelleher, C. Bonatto, G. Huyet, and S. P. Hegarty, "Excitability in optically injected semiconductor lasers: Contrasting quantum-well- and quantum-dot-based devices," Phys. Rev. E **83**, 026207 (2011).
20. B. Kelleher, S. P. Hegarty, and G. Huyet, "Modified relaxation oscillation parameters in optically injected semiconductor lasers," J. Opt. Soc. Am. B **29**, 2249–2254 (2012).
21. S. Wieczorek, B. Krauskopf, and D. Lenstra, "Multipulse excitability in a semiconductor laser with optical injection," Phys. Rev. Lett. **88**, 063901 (2002).
22. S. Wieczorek, and D. Lenstra, "Spontaneously excited pulses in an optically driven semiconductor laser," Phys. Rev. E **69**, 016218 (2004).
23. S. Wieczorek, B. Krauskopf, T. Simpson, and D. Lenstra, "The dynamical complexity of optically injected semiconductor lasers," Phys. Rep. **416**, 1–128 (2005).
24. L. Olejniczak, K. Panajotov, H. Thienpont, and M. Sciamanna, "Self-pulsations and excitability in optically injected quantum-dot lasers: Impact of the excited states and spontaneous emission noise," Phys. Rev. A **82**, 023807 (2010).
25. H. J. Wünsche, O. Brox, M. Radziunas, and F. Henneberger, "Excitability of a semiconductor laser by a two-mode homoclinic bifurcation," Phys. Rev. Lett. **88**, 023901 (2001).
26. O. Ushakov, N. Korneyev, M. Radziunas, H. J. Wünsche, and F. Henneberger, "Excitability of chaotic transients in a semiconductor laser," Europhys. Lett. **79**, 30004 (2007).
27. M. Giudici, C. Green, G. Giacomelli, U. Nespolo, and J. R. Tredicce, "Andronov bifurcation and excitability in semiconductor lasers with optical feedback," Phys. Rev. E **55**, 6414–6418 (1997).
28. J. L. A. Dubbeldam, B. Krauskopf, and D. Lenstra, "Excitability and coherence resonance in lasers with saturable absorber," Phys. Rev. E **60**, 6580 (1999).
29. J. L. A. Dubbeldam and B. Krauskopf, "Self-pulsations of lasers with saturable absorber: dynamics and bifurcations," Opt. Commun. **159**, 325–338 (1999).
30. F. Pedaci, Z. Huang, P. van Hese, S. Barland, and L. Deuker, "Excitable particles in an optical torque wrench," Nat. Phys. **7**, 259–264 (2011).
31. V. Z. Tronciu, "Excitability and coherence resonance of a DFB laser with passive dispersive reflector," Moldavian Journal of the Physical Sciences **7**, 516 (2008).
32. B. Krauskopf, K. Schneider, J. Sieber, S. Wieczorek, and M. Wolfrum, "Excitability and self-pulsations near homoclinic bifurcations in semiconductor laser systems," Opt. Commun. **215**, 367 (2003).
33. B. Romeira, J. Javaloyes, C. N. Ironside, J. M. L. Figueiredo, S. Balle, and O. Piro, "Excitability and optical pulse generation in semiconductor lasers driven by resonant tunneling diode photo-detectors," Opt. Express **21**, 20931–20940 (2013).
34. G. Hu, T. Ditzinger, C. Z. Ning, and H. Haken, "Stochastic resonance without external periodic force," Phys. Rev. Lett. **71**, 807 (1993).
35. A. S. Pikovsky, and J. Kurths, "Coherence resonance in a noise-driven excitable system," Phys. Rev. Lett. **78**, 775 (1997).
36. A. B. Neiman, P. I. Saparin, and L. Stone, "Coherence resonance at noisy precursors of bifurcations in nonlinear dynamical systems," Phys. Rev. E **56**, 270 (1997).
37. L. Gammaitoni, P. Hänggi, P. Jung, and F. Marchesoni, "Stochastic resonance," Rev. Mod. Phys. **70**, 223–287 (1998).
38. D. Ziemann, R. Aust, B. Lingnau, E. Schöll, and K. Lüdge, "Optical injection enables coherence resonance in quantum-dot lasers," Europhys. Lett. **103**, 14002 (2013).
39. G. Giacomelli, M. Giudici, S. Balle, and J. R. Tredicce, "Experimental evidence of coherence resonance in an optical system," Phys. Rev. Lett. **84**, 3298 (2000).

#206726 - $15.00 USD Received 20 Feb 2014; revised 11 Apr 2014; accepted 6 May 2014; published 27 May 2014
(C) 2014 OSA

40. F. T. Arecchi, and R. Meucci, "Stochastic and coherence resonance in lasers: homoclinic chaos and polarization bistability," Eur. Phys. J. B **67**, 93–100 (2009).
41. S. Sergeyev, K. O'Mahoney, S. Popov, and A. T. Friberg, "Coherence and anticoherence resonance in high-concentration erbium-doped fiber laser," Opt. Lett. **35**, 3736 (2010).
42. J. Hizanidis, A. G. Balanov, A. Amann, and E. Schöll, "Noise-induced front motion: signature of a global bifurcation," Phys. Rev. Lett. **96**, 244104 (2006).
43. O. V. Ushakov, H. J. Wünsche, F. Henneberger, I. A. Khovanov, L. Schimansky-Geier, and M. A. Zaks, "Coherence resonance near a Hopf bifurcation," Phys. Rev. Lett. **95**, 123903 (2005).
44. A. Zakharova, T. Vadivasova, V. Anishchenko, A. Koseska, and J. Kurths, "Stochastic bifurcations and coherencelike resonance in a self-sustained bistable noisy oscillator," Phys. Rev. E **81**, 011106 (2010).
45. A. Zakharova, A. Feoktistov, T. Vadivasova, and E. Schöll, "Coherence resonance and stochastic synchronization in a nonlinear circuit near a subcritical Hopf bifurcation," Eur. Phys. J. Spec. Top. **222**, 2481–2495 (2013).
46. N. B. Janson, A. G. Balanov, and E. Schöll, "Delayed feedback as a means of control of noise-induced motion," Phys. Rev. Lett. **93**, 010601 (2004).
47. A. G. Balanov, N. B. Janson, and E. Schöll, "Control of noise-induced oscillations by delayed feedback," Physica D **199**, 1–12 (2004).
48. S. A. Brandstetter, M. A. Dahlem, and E. Schöll, "Interplay of time-delayed feedback control and temporally correlated noise in excitable systems," Phil. Trans. R. Soc. A **368**, 391 (2010).
49. A. Vüllings, E. Schöll, and B. Lindner, "Spectra of delay-coupled heterogeneous noisy nonlinear oscillators," Eur. Phys. J. B **87**, 31 (2014).
50. C. Otto, K. Lüdge, and E. Schöll, "Modeling quantum dot lasers with optical feedback: sensitivity of bifurcation scenarios," Phys. Stat. Sol. (B) **247**, 829–845 (2010).
51. C. Otto, B. Globisch, K. Lüdge, E. Schöll, and T. Erneux, "Complex dynamics of semiconductor quantum dot lasers subject to delayed optical feedback," Int. J. Bif. Chaos **22**, 1250246 (2012).
52. R. Lang, and K. Kobayashi, "External optical feedback effects on semiconductor injection laser properties," IEEE J. Quantum Electron. **16**, 347–355 (1980).
53. R. Wetzler, A. Wacker, and E. Schöll, "Non-local Auger effect in quantum dot devices," Semicond. Sci. Technol. **19**, S43 (2004).
54. T. R. Nielsen, P. Gartner, and F. Jahnke, "Many-body theory of carrier capture and relaxation in semiconductor quantum-dot lasers," Phys. Rev. B **69**, 235314 (2004).
55. K. Lüdge, and E. Schöll, "Quantum-dot lasers – desynchronized nonlinear dynamics of electrons and holes," IEEE J. Quantum Electron. **45**, 1396–1403 (2009).
56. N. Majer, S. Dommers-Völkel, J. Gomis-Bresco, U. Woggon, K. Lüdge, and E. Schöll, "Impact of carrier-carrier scattering and carrier heating on pulse train dynamics of quantum dot semiconductor optical amplifiers," Appl. Phys. Lett. **99**, 131102 (2011).
57. B. Lingnau, K. Lüdge, W. W. Chow, and E. Schöll, "Influencing modulation properties of quantum-dot semiconductor lasers by electron lifetime engineering," Appl. Phys. Lett. **101**, 131107 (2012).
58. W. W. Chow, and S. W. Koch, *Semiconductor-Laser Fundamentals* (Springer, 1999).
59. K. Lüdge, and E. Schöll, "Nonlinear dynamics of doped semiconductor quantum dot lasers," Eur. Phys. J. D **58**, 167–174 (2010).
60. B. Globisch, C. Otto, E. Schöll, and K. Lüdge, "Influence of carrier lifetimes on the dynamical behavior of quantum-dot lasers subject to optical feedback," Phys. Rev. E **86**, 046201 (2012).
61. V. Rottschäfer, and B. Krauskopf, "The ECM-backbone of the Lang-Kobayashi equations: A geometric picture," Int. J. Bif. Chaos **17**, 1575–1588 (2007).
62. C. Grebogi, E. Ott, and J. A. Yorke, "Crises, sudden changes in chaotic attractors, and transient chaos," Physica D **7**, 181–200 (1983).
63. Y. A. Kuznetsov, *Elements of Applied Bifurcation Theory* (Springer, 1995).
64. T. Heil, I. Fischer, W. Elsäßer, and A. Gavrielides, "Dynamics of semiconductor lasers subject to delayed optical feedback: The short cavity regime," Phys. Rev. Lett. **87**, 243901 (2001).
65. T. Heil, I. Fischer, W. Elsäßer, B. Krauskopf, K. Green, and A. Gavrielides, "Delay dynamics of semiconductor lasers with short external cavities: Bifurcation scenarios and mechanisms," Phys. Rev. E **67**, 066214 (2003).
66. R. L. Stratonovich, *Topics in the Theory of Random Noise* (Gordon and Breach, 1963), vol. 1.
67. C. W. Gardiner, *Handbook of Stochastic Methods for Physics, Chemistry and the Natural Sciences* (Springer, 2002).
68. N. B. Janson, A. G. Balanov, and E. Schöll, "Delayed feedback as a means of control of noise-induced motion," Phys. Rev. Lett. **93**, 010601 (2004).
69. K. Lüdge, "Modeling quantum dot based laser devices," in *Nonlinear Laser Dynamics - From Quantum Dots to Cryptography,* [2], Chap. 1, pp. 3–34 (Wiley, 2011).
70. M. Virte, A. Karsaklian Dal Bosco, D. Wolfersberger, and M. Sciamanna, "Chaos crisis and bistability of self-pulsing dynamics in a laser diode with phase-conjugate feedback," Phys. Rev. A **84**, 043836 (2011).
71. G. Huyet, D. O'Brien, S. P. Hegarty, J. G. McInerney, A. V. Uskov, D. Bimberg, C. Ribbat, V. M. Ustinov, A. E. Zhukov, S. S. Mikhrin, A. R. Kovsh, J. K. White, K. Hinzer, and A. J. SpringThorpe, "Quantum dot

#206726 - $15.00 USD Received 20 Feb 2014; revised 11 Apr 2014; accepted 6 May 2014; published 27 May 2014
(C) 2014 OSA

semiconductor lasers with optical feedback," phys. stat. sol. (b) **201**, 345–352 (2004).
72. M. Radziunas, A. Glitzky, U. Bandelow, M. Wolfrum, U. Troppenz, J. Kreissl, and W. Rehbein, "Improving the Modulation Bandwidth in Semiconductor Lasers by Passive Feedback," IEEE J. Sel. Top. Quantum Electron. **13**, 136–142 (2007).
73. A. Argyris, M. Hamacher, K. E. Chlouverakis, A. Bogris, and D. Syvridis, "Photonic integrated device for chaos applications in communications," Phys. Rev. Lett. **100**, 194101 (2008).
74. B. Haegeman, K. Engelborghs, D. Roose, D. Pieroux, and T. Erneux, "Stability and rupture of bifurcation bridges in semiconductor lasers subject to optical feedback," Phys. Rev. E **66**, 046216 (2002).
75. K. Green, "Stability near threshold in a semiconductor laser subject to optical feedback: A bifurcation analysis of the Lang-Kobayashi equations," Phys. Rev. E **79**, 036210 (2009).
76. E. Schöll, *Nonequilibrium Phase Transitions in Semiconductors* (Springer, Berlin, 1987).
77. T. Erneux, and P. Glorieux, *Laser Dynamics* (Cambridge University Press, UK, 2010).

1. Introduction

Semiconductor quantum dot (QD) lasers [1, 2] are promising candidates for optical communication applications and high-speed data transmission, since they are singled out by a narrow linewidth [1] due to small phase-amplitude coupling [3–5], and by strongly suppressed relaxation oscillations. The latter can be attributed to the special carrier scattering dynamics of QD lasers [6, 7]. It results in an higher dynamical stability of these lasers with respect to perturbation, e.g., external optical injection [8] or optical feedback [9]. This results in simpler bifurcation scenarios and therefore in a better observability of nonlinear effects in experiments, which will be crucial for the noise induced dynamics discussed in this paper.

Understanding noise-induced effects, e.g., due to spontaneous emission noise, is indispensable for a variety of semiconductor devices, to name just a few: the performance of QD optical amplifiers [10], the polarization dynamics of surface emitting lasers [11] or the synchronization properties of coupled laser systems [12, 13]. A special situation emerges for devices that can be operated as excitable systems, i.e., systems that rest in a stable steady state, but can be excited to emit a spike by a super-threshold perturbation (e.g. noise). Well-known examples for excitable systems are spiking neurons [14], cardiac dynamics [15], and nonlinear chemical reactions [16]. Excitability in laser systems received considerable interest in the last years. It was observed experimentally [17–20] and studied theoretically [21–24] in lasers with optical injection. Furthermore, excitability was found in lasers with short optical feedback [25, 26] as well as in lasers with a long external cavity [27], and it was investigated theoretically in lasers with saturable absorbers [28, 29].

Recently, it has been demonstrated that an excitable optical unit may be used as an optical tongue wrench permitting to sense single perturbation events [30]. Data transmission systems based on excitable optical units confer a high degree of robustness due to their inherent signal reshaping capabilities. Therefore, it has been suggested to use an excitable optical unit as optical switch for all-optical-signal processing where it only reacts on sufficiently high optical input signals [31] or for noise reduction in optical telecommunication applications [32]: a noisy input pulse triggers a "clean" output pulse. Generation of nanosecond pulses by an excitable semiconductor laser in an integrated optoelectronic circuits was already experimentally demonstrated [33]. However, in the conventional setup of a quantum well (QW) semiconductor laser under long external optical feedback bifurcation points lie very dense. This makes it hard to experimentally address the small regions of excitability, which occur only close to certain bifurcation points. Instead, the QD laser with short optical feedback studied in this paper is dynamically more stable, and showing a simpler bifurcation scenario, it is thus more promising for this kind of application.

The counter-intuitive effect that an increase of the noise can lead to an increase of correlation, i.e., to an increase of the regularity of the spikes observed in the excitable regime, is known as coherence resonance [34–36]. In contrast to stochastic resonance (see [37] for a review) the

#206726 - $15.00 USD Received 20 Feb 2014; revised 11 Apr 2014; accepted 6 May 2014; published 27 May 2014
(C) 2014 OSA

effect occurs without periodic forcing of the system. Coherence resonance is already an intensively studied effect and was shown theoretically in quantum well (QW) lasers with saturable absorber [28], in QD lasers under optical injection [38], in lasers subject to long optical feedback [32, 39], in laser systems with polarization instabilities [40, 41], in semiconductor superlattices [42], as well as in non-excitable systems below a subcritical Hopf-bifurcation [43–45].

In this paper, excitability and coherence resonance close to a boundary crisis bifurcation found in a QD laser subject to short optical feedback are studied. It is known that coherence resonance can be controlled by delayed feedback, e.g. for neural systems in the framework of the FitzHugh-Nagumo model (type-II excitability) [46–48], for systems close to a saddle-node infinite period bifurcation (type-I excitability), and close to a subcritical Hopf-bifurcation [49], however so far it has not been investigated close to a boundary crises. Using a sophisticated microscopically motivated rate equation approach, we show that the interesting effect of tunable regularity of emitted spikes strongly depends on the operating pump current and is thus easily accessible in experiments.

The paper is structured as follows: At first, in Sec. 2 a dimensionless version of the dynamic equations is introduced and the structure of the basic continuous wave (cw) solutions is discussed. Next, in Sec. 3 the bifurcation structure of the deterministic system is analyzed and its dynamics in the bistable regimes close to the loci of the bifurcation points, which render the system excitable, is studied in detail. Then, in Sec. 4 coherence resonance of the system subject to Gaussian white spontaneous emission noise is discussed in dependence of the pump current, before concluding in Sec. 4. Eventually, in Appendix A the dimensionless version of the model equations is derived.

2. Quantum dot laser model

The microscopically based rate equation model for the QD laser under optical feedback was previously discussed in [9, 50, 51]. Here a dimensionless form of the dynamical equations is used, which is derived in Appendix A. A sketch of the edge-emitting single-mode laser device

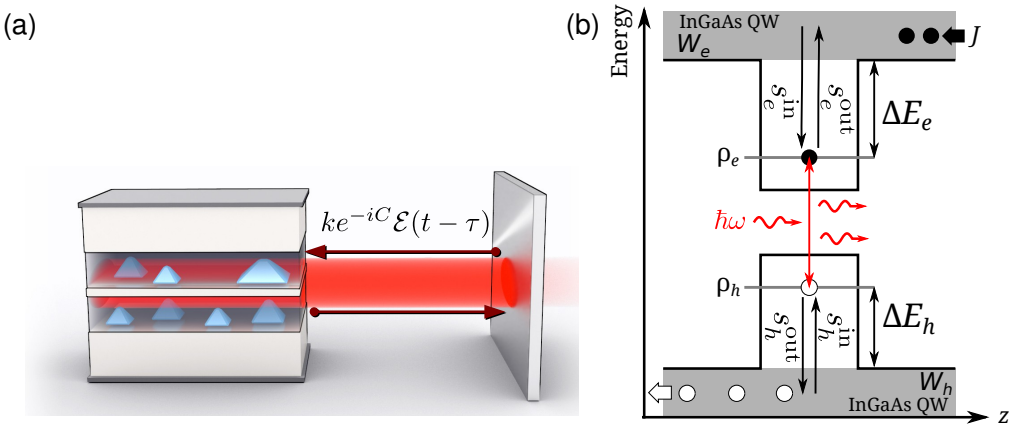

Figure 1. **(a)**: Sketch of the laser under delayed optical feedback. **(b)**: Sketch of band structure.

is shown in Fig. 1(a). The light in the cavity is modeled by a semiclassical Lang-Kobayashi-type [52] equation for the slowly varying complex amplitude $\mathscr{E}$ of the electric field. Taking into account only one roundtrip of the light in the external cavity, the field amplitude $\mathscr{E}(t-\tau)$ delayed by the external cavity roundtrip time τ is coupled back into the laser with feedback strength k and rotated by the external cavity phase C.

#206726 - $15.00 USD Received 20 Feb 2014; revised 11 Apr 2014; accepted 6 May 2014; published 27 May 2014
(C) 2014 OSA

The energy-band diagram of the dot-in-a-well structure under consideration is sketched in Fig. 1(b). The carriers are first injected in the InGaAs quantum well (QW), which acts as a carrier reservoir, with the dimensionless pump rate J. Within the QDs formed by pyramidal structures of InGaAs, localized, discrete electron and hole ground states are considered that lead to a wavelength of the optical transition of $\lambda_{\mathrm{opt}} = 1.3\mu\mathrm{m}$. The occupation probabilities of electrons and holes in these states are denoted by ρ_e and ρ_h, respectively.

Coulomb scattering (nonlocal Auger scattering) is the dominating scattering process for high carrier densities in the lasing regime [53]. Therefore, electron-phonon scattering is neglected for the carrier exchange between QW and QDs, but it is taken into account for the intraband transitions within the carrier reservoir. In the model the carrier exchange between QW and QDs is mediated by non-constant microscopically calculated Coulomb in- ($s^{\mathrm{in}}_{e/h}$) and out-scattering ($s^{\mathrm{out}}_{e/h}$) rates [54–56], which are nonlinear functions of the dimensionless carrier densities of electrons (W_e) and holes (W_h) in the carrier reservoir, and therefore depend on J. Note, that we use only dimensionless quantities for the rates (details of the non-dimensionalization can be found in [7, 51]). The scattering rates also strongly depend on the energy spacings between the QW band edges and the discrete QD levels, which are given by $\Delta E_e = 210\,\mathrm{meV}$ and $\Delta E_h = 50\,\mathrm{meV}$ for electrons and holes, respectively. The latter strongly depend on the size of the QDs and also on their material composition. In comparison to conventional QW lasers the carrier lifetimes $\tau_{e/h}$ (in their dimensionless form $t_{e/h} = \tau_{e/h} W \equiv (s^{\mathrm{in}}_{e/h} + s^{\mathrm{out}}_{e/h})^{-1}$ with $W = 0.7ns^{-1}$ being the Einstein coefficient of spontaneous emission) constitute additional timescales, which are responsible for the strong suppression of the relaxation oscillations (ROs) of QD lasers [57] mentioned in the introduction. The order of magnitude of τ_e and τ_h can be tuned by the pump current J, which permits to tune the turn-on damping of the laser.

In the subsystem of the carriers, different dynamics is taken into account for ρ_e and ρ_h as well as for W_e and W_h. Therefore, the system of coupled delay differential equations reads

$$\mathscr{E}'(t') = \frac{1+i\alpha}{2}\Big[g(\rho_e+\rho_h-1)-1\Big]\mathscr{E}(t') + k e^{iC}\mathscr{E}(t'-\tau) + \sqrt{\beta r_{\mathrm{sp}}\rho_e\rho_h}\,\xi(t'), \tag{1a}$$

$$\rho_e' = \gamma\Big[F_e - r_w(\rho_e+\rho_h-1)\big|\mathscr{E}\big|^2 - \rho_e\rho_h\Big], \tag{1b}$$

$$\rho_h' = \gamma\Big[F_h - r_w(\rho_e+\rho_h-1)\big|\mathscr{E}\big|^2 - \rho_e\rho_h\Big], \tag{1c}$$

$$W_e' = \gamma\Big[J - F_e - cW_eW_h\Big], \tag{1d}$$

$$W_h' = \gamma\Big[J - F_h - cW_eW_h\Big]. \tag{1e}$$

Here, time $t' \equiv t/\tau_{\mathrm{ph}}$ is rescaled with respect to the photon lifetime τ_{ph}, where t denotes the physical time, and $(\cdot)'$ denotes the derivative respect to t'. The amplitude-phase coupling is modeled by a constant linewidth enhancement factor α to admit analytical insight. Note however, that the validity of this approach depends upon the band structure under consideration. In general, the α-factor is not a reliable parameter in QD lasers as shown recently in [4, 5]. The α-factor is defined as the variation of the real refractive index, which is proportional to the real part of the complex susceptibility with the carrier density divided by the variation of the gain, which is proportional to the imaginary part of the complex susceptibility, with the carrier density. However, each charge carrier transition in the band structure under consideration contributes differently to the complex susceptibility. While the resonant transitions of the QD carriers mainly affect the gain, the main contribution to the change of the refractive index is given by the off resonant carriers of the surrounding carrier reservoir (QW) (see [4] for de-

#206726 - $15.00 USD Received 20 Feb 2014; revised 11 Apr 2014; accepted 6 May 2014; published 27 May 2014
(C) 2014 OSA

Table 1. Parameter values used in the numerical simulations.

Symbol	Value	Meaning
g	3.96	Linear gain parameter
γ	7×10^{-3}	Ratio of photon to carrier lifetime
τ	16	External cavity round-trip time
c	1.54	Spontaneous and non-radiative losses
α	0.9	Linewidth enhancement factor
r_{sp}	1.26×10^4	Coefficient of spontaneous emission
C	π	External cavity phase
r_w	$1.5 \cdot 10^{-4}$	Ratio of Einstein coefficients of induced and spontaneous emission

tails). For shallow QDs the timescale of the intensity pulsations, which are, as the ROs, on the timescale of nano-seconds, is large compared to the timescale of the carrier exchange between QW and QDs (given by τ_e and τ_h). The carrier exchange is then fast enough to synchronize QD and QW carriers, and the approximation of a constant α-factor holds. But, for very deep dots the carrier exchange between QD and QW can become so slow that it takes place on a similar timescale than the intensity pulsations. As a result, QDs and QW carriers can become desynchronized in feedback regimes, in which intensity pulsations are observed. In this regimes, the approximation of a constant α-factor then fails. Nevertheless, for the band structure discussed in this paper, the approximation of a constant α-factor yields reliable results.

The linear gain coefficient is denoted by g. The value of g takes into account that due to the inhomogeneous broadening of the gain medium only a subgroup of all QDs matches the mode energies for lasing. Further, the rescaled feedback strength is denoted by $k \equiv K\tau_{\mathrm{ph}}/\tau_{\mathrm{in}}$, where K is the dimensionless feedback strength ranging from zero to one (see Appendix A), τ_{in} is the roundtrip time of the light in the internal cavity, and the dimensionless roundtrip time of the light in the external cavity is given by τ. The process of spontaneous emission is modeled by a complex Gaussian white noise term $\xi(t')$, i.e.,

$$\xi(t') = \xi_a(t') + i\xi_b(t'), \quad \langle \xi_i(t') \rangle = 0,$$
$$\langle \xi_a(t')\xi_b(\tilde{t}') \rangle = \delta_{a,b}\delta(t-\tilde{t}'), \quad \text{for} \quad \xi_i(t') \in \mathbb{R}, i \in \{a,b\}.$$

Here, subscripts a and b stand for real and imaginary parts, respectively. The spontaneous emission factor β measures the probability that a spontaneously emitted photon is emitted into the lasing mode. This will be the important parameter to vary the noise strength. The rate of the spontaneous emission is given by $r_{\mathrm{sp}} \equiv Z_a^{\mathrm{QD}} W \tau_{\mathrm{ph}}$, where Z_a^{QD} is the number of QDs that are resonant with the optical transition, and W is the Einstein factor of the spontaneous emission resulting from the incoherent interaction of the QDs with all resonator modes [58]. The small parameter γ multiplying the right hand sides of Eqs. (1b)–(1e) expresses the timescale separation between the fast field equation and the slow subsystem of the carriers. The terms $F_{e/h} \equiv s^{\mathrm{in}}_{e/h}(W_e, W_h)(1-\rho_{e/h}) - s^{\mathrm{out}}_{e/h}(W_e, W_h)\rho_{e/h}$ model the contributions of the scattering rates, where the Pauli blocking is described by the terms $1-\rho_{e/h}$. In- and out-scattering rates are related by a detailed balance relations [55, 59]. Fit functions for $s^{\mathrm{in}}_{e/h}$ can be found in Ref. [60]. Further, r_w describes the ratio of the Einstein coefficients of induced and spontaneous emission, which was denoted by w in Ref. [60], and c is the band-band recombination coefficient in the QW. Parameter values used in the simulations are given in Tab. 1.

It is crucial to note for the subsequent analysis that the carrier equations (1b)–(1e) are not independent but contain carrier conservation, which can be seen by verifying that $\rho_e' + W_e' =$

#206726 - $15.00 USD Received 20 Feb 2014; revised 11 Apr 2014; accepted 6 May 2014; published 27 May 2014
(C) 2014 OSA

$\rho_h' + W_h'$ holds. Thus, $\rho_e - \rho_h + W_e - W_h$ is a constant, which is zero in the intrinsic case [59]. Due to the carrier conservation, one dynamical variable can be eliminated by expressing one carrier type in terms of the others, i.e.,

$$W_h = \rho_e + W_e - \rho_h. \tag{2}$$

2.1. *External cavity modes–stationary solutions*

In this section, the basic solutions of the dynamical equations (1) without noise ($\beta = 0$) are discussed. These external cavity modes (ECMs) organize the phase space of the system and provide a "backbone" for more complex, e.g., chaotic, dynamics observed in these systems [61], and therefore it is crucial to understand their bifurcation structure. They are cw solutions with constant photon number $N_{\mathrm{ph}} = N_{\mathrm{ph}}^{\mathrm{s}}$ and carrier densities $\rho_{e/h}^{\mathrm{s}}, W_{e/h}^{\mathrm{s}}$, and a phase $\phi \equiv \delta\omega^{\mathrm{s}} t$ of the electric field amplitude $\mathscr{E} \equiv \sqrt{N_{\mathrm{ph}}} e^{i\phi}$ that varies linearly in time

$$\left(\mathscr{E}, \rho_{e/h}, W_{e/h}\right) = \left(\sqrt{N_{\mathrm{ph}}^{\mathrm{s}}} e^{i\delta\omega^{\mathrm{s}} t'}, \rho_{e/h}^{\mathrm{s}}, W_{e/h}^{\mathrm{s}}\right), \tag{3}$$

where the steady states of the dynamic equations (1) with feedback are denoted by the superscript s, and $\delta\omega^{\mathrm{s}} \equiv \tau_{\mathrm{ph}}(\omega - \omega_{\mathrm{th}})$ is the deviation of the frequency ω of the ECM from the threshold frequency of the solitary laser ω_{th}. Inserting the ECM-ansatz (3) into Eqs. (1), we find the following expressions for the non-zero intensity solutions ($N_{\mathrm{ph}}^{\mathrm{s}} \neq 0$)

$$\rho_{\mathrm{inv}}^{\mathrm{s}} = -k\cos(\delta\omega^{\mathrm{s}}\tau + C), \tag{4a}$$
$$\delta\omega^{\mathrm{s}} = \alpha\rho_{\mathrm{inv}}^{\mathrm{s}} - k\sin(\delta\omega^{\mathrm{s}}\tau + C), \tag{4b}$$
$$0 = \gamma\left[F_e^{\mathrm{s}} - r_w(\rho_e^{\mathrm{s}} + \rho_h^{\mathrm{s}} - 1)N_{\mathrm{ph}}^{\mathrm{s}} - \rho_e^{\mathrm{s}}\rho_h^{\mathrm{s}}\right], \tag{4c}$$
$$0 = \gamma\left[F_h^{\mathrm{s}} - r_w(\rho_e^{\mathrm{s}} + \rho_h^{\mathrm{s}} - 1)N_{\mathrm{ph}}^{\mathrm{s}} - \rho_e^{\mathrm{s}}\rho_h^{\mathrm{s}}\right], \tag{4d}$$
$$0 = J - F_e^{\mathrm{s}} - cW_e^{\mathrm{s}}W_h^{\mathrm{s}}, \tag{4e}$$
$$0 = J - F_h^{\mathrm{s}} - cW_e^{\mathrm{s}}W_h^{\mathrm{s}}, \tag{4f}$$

where a rescaled inversion

$$\rho_{\mathrm{inv}} \equiv \frac{1}{2}\left[g(\rho_e + \rho_h - 1) - 1\right] \tag{5}$$

has been introduced. Inserting Eq. (4a) into Eq. (4b), we obtain a transcendental equation for $\delta\omega^{\mathrm{s}}$ in terms of α, τ, and C

$$\delta\omega^{\mathrm{s}} = -k_{\mathrm{eff}}\sin\left(\delta\omega^{\mathrm{s}}\tau + C + \arctan(\alpha)\right), \tag{6}$$

where $k_{\mathrm{eff}} \equiv k\tau\sqrt{1+\alpha^2}$. For $k_{\mathrm{eff}} < 1$ only one solution exists, and at $k_{\mathrm{eff}} = 1$ a pair of ECMs is created in a saddle-node bifurcation. Increasing k, α, and τ additional pairs of solutions are created in saddle-node bifurcations. The saddle solutions (anti-modes) are always unstable and the stability of the node solutions (modes) has to be determined by a linear stability analysis [51]. Taking advantage of the carrier conservation (Eq. (2)), we can reformulate Eq. (4a) to express ρ_e^{s} and ρ_h^{s} in terms of W_e^{s} and W_h^{s}

$$\rho_e^{\mathrm{s}} = \frac{1}{2}\left[\frac{1 + g - 2k\cos(\delta\omega^{\mathrm{s}} + C)}{g} + W_h^{\mathrm{s}} - W_e^{\mathrm{s}}\right], \tag{7a}$$
$$\rho_h^{\mathrm{s}} = \frac{1}{2}\left[\frac{1 + g - 2k\cos(\delta\omega^{\mathrm{s}} + C)}{g} + W_e^{\mathrm{s}} - W_h^{\mathrm{s}}\right]. \tag{7b}$$

#206726 - $15.00 USD Received 20 Feb 2014; revised 11 Apr 2014; accepted 6 May 2014; published 27 May 2014
(C) 2014 OSA

Further, an expression for $N_{\rm ph}^{\rm s}$ as a function of the carrier populations can be obtained, by inserting the sum of Eqs. (4c) and (4d) into the sum of Eqs (4e) and (4f)

$$\begin{aligned} N_{\rm ph}^{\rm s} &= \frac{g}{r_w\big(1-2k\cos(\delta\omega^{\rm s}+C)\big)}\big[J-\rho_e^{\rm s}\rho_h^{\rm s}-cW_e^{\rm s}W_h^{\rm s}\big] \\ &= \frac{g}{r_w\big(1-2k\cos(\delta\omega^{\rm s}+C)\big)}\big[J-J_{\rm th}\big], \end{aligned} \tag{8}$$

where the pump current at lasing threshold $J_{\rm th}\equiv\rho_e^{\rm s}\rho_h^{\rm s}-cW_e^{\rm s}W_h^{\rm s}$ has been introduced in the second line. Eventually, the steady states $W_e^{\rm s}$ and $W_h^{\rm s}$ may be determined by solving Eqs. (4e) and (4f) self-consistently, which has to be done numerically, because $s_{e/h}^{\rm in/out}=s_{e/h}^{\rm in/out}(W_e,W_h)$ are nonlinear functions of W_e and W_h.

3. Bifurcation structure and excitable dynamics

To understand the noise induced excitations, we first have to characterize the bifurcation structure of the deterministic system, and we then have to discuss which phase space configurations lead to excitability. In principle, this structure was already reported elsewhere, [50, 51, 60]. Here, we focus on the dependence of the bifurcations on the pump current, which is crucial for the discussion of the excitable dynamics. Figures 2(a) and 2(c) depict the bifurcation diagrams of the local maxima of $N_{\rm ph}$ versus feedback strength K for low $J=2J_{\rm th}$ (red dots) and for higher $J=3J_{\rm th}$ (black dots) and $J=4J_{\rm th}$ (gray dots), respectively. Note that for the subsequent discussion we use the feedback strength K, which is more intuitive because it ranges from zero to one. The bifurcation diagrams have been obtained by increasing K stepwise using in each step the last τ-interval of the time series of the previous run as initial condition. Figure 2(b) depicts the frequency deviation $\delta\omega^{\rm s}$ of the ECMs. Solid and dashed lines indicate stable and unstable solutions, respectively. For low K, only one ECM (blue line) exists, which initially is stable. For $J=2J_{\rm th}$ this ECM is destabilized in a supercritical Hopf bifurcation at $K_H(J=2J_{\rm th})=0.085$ (red dot in Fig. 2(b)), which results in a stable solution with a periodically modulated $N_{\rm ph}$ (see leftmost inset in Fig. 2(a)). Increasing K further, this periodic orbit undergoes a cascade of period doubling bifurcations. After a large period-2 window, the system becomes chaotic at $K=0.21$ (see middle inset in Fig. 2(a) for a time series of $N_{\rm ph}$). At the end of the region with complex dynamics, the chaotic attractor collapses onto a limit cycle, and periodic pulse packages are observed in the time series of $N_{\rm ph}$, which will be discussed in detail below (see rightmost inset in Fig. 2(a)). At $K_{\rm sn}=0.2290$ a new pair of ECMs is created at in a saddle-node bifurcation (limit point) indicated by an open black circle in Fig. 2(b). The position of the limit point is determined by Eq. (6) only, and is thus independent of J. In Fig. 2(b), the stable 2$^{\rm nd}$ ECM is depicted by a green and the unstable anti-mode by a black dashed line. The photon number $N_{\rm ph}^{\rm s}$ of the stable parts of the first and the 2$^{\rm nd}$ ECMs and of the unstable anti-mode are plotted in Figs. 2(a) and 2(c), by thick blue, thick green, and black dashed lines, respectively. For $J=2J_{\rm th}$, bi-stability between the periodic orbit and the 2$^{\rm nd}$ ECM is observed upon its creation at $\rm K_{sn}$, until eventually at $K_{\rm hom}=0.22920$, the periodic orbit is annihilated in a homoclinic bifurcation (brown vertical arrow) with the saddle (anti-mode) of the 2$^{\rm nd}$ ECM-pair. For $K>K_{\rm hom}$, the laser emits in stable cw operation on the 2$^{\rm nd}$ ECM.

With varying current, the bifurcation scenario changes. In Ref. [7], it was shown that the RO damping increases linearly with the pump current. This is the reason why for higher $J=3J_{\rm th}$ and $J=4J_{\rm th}$, the Hopf-bifurcation points K_H shift toward higher K-values [9] (red dots and blue arrows in Fig. 2(b). Further, for pump currents larger than $J>2.8J_{\rm th}$ the end of the bifurcation cascade is not marked by a homoclinic bifurcation, but by a boundary crisis [62] of the chaotic attractor that collides at $K_{\rm cris}$ with the saddle (anti-mode) of the 2$^{\rm nd}$ ECM pair. Bi-stability is now observed in the interval $[\rm K_{sn}, K_{cris}]$. The feedback strengths $K_{\rm hom}$ and $K_{\rm cris}$, at which

#206726 - $15.00 USD Received 20 Feb 2014; revised 11 Apr 2014; accepted 6 May 2014; published 27 May 2014
(C) 2014 OSA

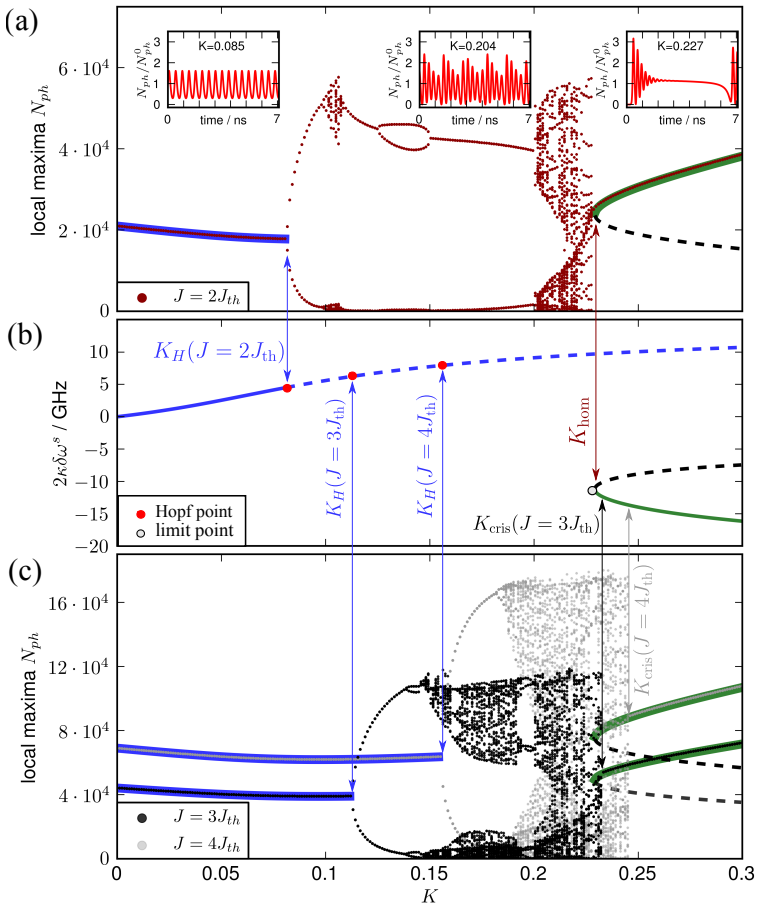

Figure 2. Deterministic dynamics: **(a)**: Bifurcation diagram of local maxima of photon number $N_{\rm ph}$ vs. feedback strength K for pump current $J = 2J_{\rm th}$ (brown dots), where $J_{\rm th}$ ist the threshold current. Thick blue and green lines denote the steady state photon numbers $N_{\rm ph}^{\rm s}$ of the stable parts of the first and the second ECM, respectively, and the black dashed line denotes $N_{\rm ph}^{\rm s}$ of the unstable antimode. Insets show time traces of $N_{\rm ph}$ for fixed K. **(b)**: Frequency deviations $\delta\omega^{\rm s}$ of the ECMs vs. K. Solid and dashed lines denote stable and unstable solutions, respectively. Hopf and limit points are denoted by red dots and open black circles, respectively. Blue, red, and black (gray) arrows indicate the feedback strengths of the Hopf points (K_H), the homoclinic bifurcation ($K_{\rm hom}$), and the boundary crisis ($K_{\rm cris}$), respectively. **(c)**: Same as **(a)** but for higher $J = 3J_{\rm th}$ (black dots) and $J = 4J_{\rm th}$ (gray dots). Parameters as in Table 1.

#206726 - $15.00 USD Received 20 Feb 2014; revised 11 Apr 2014; accepted 6 May 2014; published 27 May 2014
(C) 2014 OSA

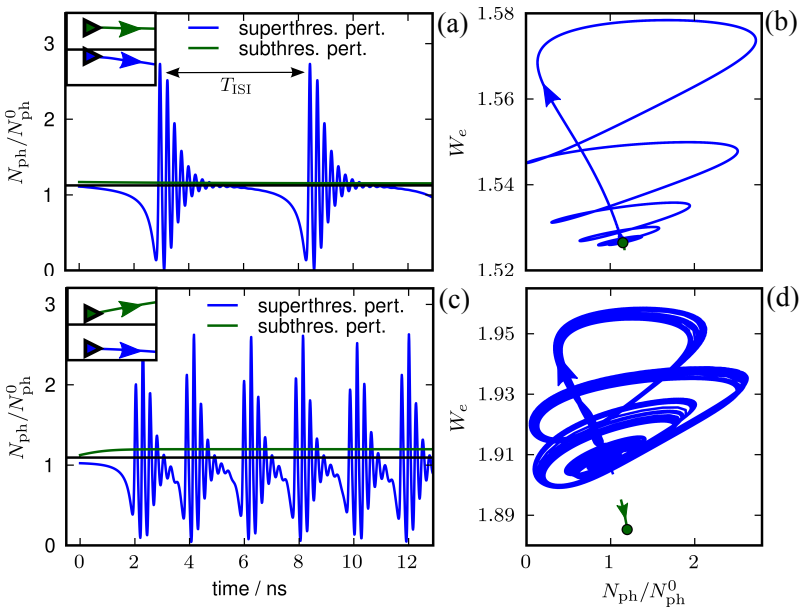

Figure 3. Subthreshold (green lines) and super-threshold (blue lines) excitations of deterministic system in the bistable regime. **(a)** and **(b)**: Close to a homoclinic bifurcation for $K = 0.229$ and $J = 2J_{\mathrm{th}}$. **(c)** and **(d)**: Close to a boundary crisis of chaotic attractor for $K = 0.23$ and $J = 3J_{\mathrm{th}}$. Blue and green triangles in the closeups mark the starting points of the perturbed trajectories for super- and subthreshold perturbations, respectively. Black lines denote the steady state photon number of the unstable anti-mode of the 2nd ECM-pair. **(a)** and **(c)**: Time series of the perturbed trajectories. **(b)** and **(d)**: Projections of the trajectories onto the (N_{ph}, W_e)-plane. Green dots indicate the position of the stable 2nd ECM-mode. Parameters as in Table 1.

homoclinic bifurcation and boundary crisis occur, have been found by up- and down-sweeping K with a very small stepsize of $\Delta K = 1 \cdot 10^{-5}$. For up-sweeping K, the system remains on the periodic orbit (chaotic attractor), up to K_{hom} (K_{cris}), while for down-sweeping K the laser emits on the 2nd ECM down to K_{sn}. Therefore, K_{hom} and K_{cris} are determined by the upper limit of the bi-stability region. In contrast to the homoclinic bifurcation that is independent of the pump current for $J \in [J_{\mathrm{th}}, 2.8J_{\mathrm{th}}]$, the feedback strength K_{cris}, at which the boundary crisis occurs, increases with the pump current (see dark and light arrow in Fig. 2(c)).

The laser is excitable for K-values little larger than K_{hom} for $J < 2.8J_{\mathrm{th}}$ and analogously for K-values little above K_{cris} for $J > 2.8J_{\mathrm{th}}$. In both cases, the short unstable manifold of the anti-mode acts as perturbation threshold. For $J \leq 2.8J_{\mathrm{th}}$, the response of the system to a super-threshold perturbation is a large excursion of the trajectory in phase space close to the "ghost" of the limit-cycle that is destroyed in the homoclinic bifurcation. For $J > 2.8J_{\mathrm{th}}$, the excursion in phase space is guided by the ruin of the chaotic attractor that collapses at K_{cris}. In Figs. 2(a) and 2(c) this situation is elucidated, the threshold is given by the difference of the photon numbers $N^{\mathrm{s}}_{\mathrm{ph}}$ of the 2nd ECM (thick green line) and of the anti-mode (black dashed line). The threshold is very low for $K = K_{\mathrm{hom}}$ and increases with K. This implies that for $J > 2.8J_{\mathrm{th}}$, when the system re-stabilizes in a boundary crisis, the threshold can be tuned by varying the pump current and with it the critical feedback strength $K_{\mathrm{cris}} = K_{\mathrm{cris}}(J)$.

Next, the dynamics in phase space is discussed to gain a better understanding of the difference between the excitable behavior close to the homoclinic bifurcation and close to a boundary

#206726 - $15.00 USD Received 20 Feb 2014; revised 11 Apr 2014; accepted 6 May 2014; published 27 May 2014
(C) 2014 OSA

crisis. Figures 3(a) and 3(b) depict time series and phase space projections onto the (N_{ph}, W_e)-plane for $K = 0.2290$, i.e., just below K_{hom}, where the periodic orbit still exists. A subthreshold perturbation of the system from the stable 2nd ECM, i.e, the lasing fixed point, (green line) decays rapidly back to this steady state, while a super-threshold perturbation (blue line) yields strictly periodic pulse package, i.e., a motion along the periodic orbit. The green and the blue triangles in the closeup of Fig. 3(a) denote the starting point of the trajectories and the photon number of the anti-mode is plotted as a black line. In Ref. [50] we showed that the inter-pulse interval time T_{ISI} scales logarithmically with the distance from the bifurcation point, i.e., $T_{\mathrm{ISI}} \sim \ln|K - K_{\mathrm{hom}}|$, as it is expected close to a homoclinic bifurcation [63]. In the phase space projection in Fig. 3(b), it can be seen that after a power dropout at the end of each pulse package (nearly vertical part of the trajectory), the trajectory at first performs pronounced damped oscillations spiraling around the point in phase space, where the 2nd pair of ECMs has been created at the nearby saddle-node bifurcation (the green dot in Fig. 3(b) indicates the stable 2nd ECM). Afterwards, it is re-injected into the high gain region during the power dropout.

The lower panel of Fig. 3 depicts the excitability of the laser close to the boundary crisis for $K = 0.23$, which is a little below $K_{\mathrm{cris}}(J = 3)$. A super-threshold perturbation (blue line in Fig. 3(d)) yields rather regular pulse packages, although they are not strictly periodic as the ones observed close to the homoclinic bifurcation. Furthermore, the inter-spike interval time does not obey a specific scaling law as the pulse packages described before. From the phase space projection in Fig. 3(b), we see that the trajectory has essentially the same shape observed close to the homoclinic bifurcation, but does not close up, which yields a certain width of the chaotic attractor in phase space. Note that these regular pulse packages are similar to those observed by Heil et al. in a QW laser with short optical feedback [64, 65]. Comparing the distance of $N_{\mathrm{ph}}^{\mathrm{s}}$ of the 2nd ECM (green line) and $N_{\mathrm{ph}}^{\mathrm{s}}$ of the anti-mode (black line) in Figs. 3(a) and 3(c), we see that the excitation threshold is much larger close to the crisis than close to the homoclinic bifurcation. Thus, close to the crisis larger perturbations (higher noise levels) are needed to excite the system and cause a phase space excursion.

4. Coherence resonance

In this section, we analyze the phenomenon of coherence resonance close to the end of the first bifurcation cascade discussed in the previous section. As a measure for the regularity of the pulse packages, the correlation time t_{cor} is used. For a stationary stochastic process y, it was introduced by Stratonovich [66] as

$$t_{\mathrm{cor}} \equiv \int_{\mathbb{R}_0^+} |\Psi_y(s)| ds, \tag{9}$$

where $\Psi_y \equiv \frac{1}{\sigma_y^2}\langle (y(t-s) - \langle y\rangle)(y(t) - \langle y\rangle)\rangle$. Here, Ψ_y denotes the normalized autocorrelation function of y, $\langle\cdot\rangle$ denotes the ensemble average, and the variance is given by $\sigma_y^2 \equiv \Psi_y(0) = \langle (y(t) - \langle y\rangle)^2\rangle$. Using the Wiener-Khinchin theorem, which states that power spectral density and autocorrelation function are a Fourier-pair [67], we calculate Ψ_y from the ensemble averaged power spectral density. Here, we take the photon number as stochastic process, i.e., $y = N_{\mathrm{ph}}$. Another measure for the regularity of the pulse packages is the normalized standard deviation of the inter-spike interval time T_{ISI} [68]

$$R_T \equiv \frac{\sqrt{\langle T_{\mathrm{ISI}}^2\rangle - \langle T_{\mathrm{ISI}}\rangle^2}}{\langle T_{\mathrm{ISI}}\rangle}, \tag{10}$$

which is also known as normalized fluctuations [35]. In our laser system, the noise is applied only to the optical equations. Therefore, measuring T_{ISI} not directly from the timeseries of N_{ph}

#206726 - $15.00 USD Received 20 Feb 2014; revised 11 Apr 2014; accepted 6 May 2014; published 27 May 2014
(C) 2014 OSA

but from the carrier inversion yields more robust results, because the latter are only indirectly effected by the noise. The dropout of N_{ph} before the first intensity spike of each pulse package (cf. Fig. 3(a)) corresponds to a spike of the inversion ρ_{inv} defined in Eq. (5), which is followed by a damped oscillation towards its steady state value $\rho_{\mathrm{inv}}^{\mathrm{s}}$. To determine T_{ISI}, a threshold value $\rho_{\mathrm{inv}}^{\mathrm{thr}} = 0.1$ is chosen, which is crossed during the first dropout of each pulse package, but not during the subsequent damped oscillations. To find the exact timing position of the first spike of the inversion of the n-th pulse package, we define a probability density by

$$\rho_n(t') \equiv \frac{\rho_{\mathrm{inv}}^2(t')}{\rho_{\mathrm{inv},n}}, \quad \text{with} \quad \rho_{\mathrm{inv},n} \equiv \int_{t'_{n,b}}^{t'_{n,e}} \rho_{\mathrm{inv}}^2(\tilde{t})d\tilde{t},$$

where $t'_{n,b}$ denotes the time when the leading edge of the n-th pulse first exceeds the threshold $\rho_{\mathrm{inv}}(t'_{n,b}) > \rho_{\mathrm{inv}}^{\mathrm{thr}}$, and $t'_{n,e}$ denotes the time when the trailing edge of the pulse first falls below the threshold value, i.e., $\rho_{\mathrm{inv}}(t'_{n,e}) < \rho_{\mathrm{inv}}^{\mathrm{thr}}$. The timing position of the first spike of the n-th pulse package is then determined by the first moment (mean) of the distribution function $\rho_n(t')$

$$t'_n \equiv \int_{t'_{n,b}}^{t'_{n,e}} \rho_n(\tilde{t})\,\tilde{t}\,d\tilde{t}.$$

Eventually, the sequence of inter-spike intervals T_{ISI}, from which R_T is calculated, is defined by the difference of the timing positions of the first spikes of subsequent pulse packages. For the chaotic system, we take advantage of the special shape of the chaotic attractor. The trajectory is nearly periodic, meaning that the height of the first spikes of the pulse packages varies little compared to the height difference of the first and the second spike of each pulse package (cf. Figs. 3(c) and 3(d)). Therefore, for the deterministic system it is always possible to find an appropriate threshold value $\rho_{\mathrm{inv}}^{\mathrm{thr}}$, that is only passed by the first spike of each pulse package.

To study coherence resonance, the QD laser is operated on the stable 2$^{\mathrm{nd}}$ ECM just behind the bifurcation cascade, where the deterministic system is not bistable anymore. For instance, this implies that the deterministic system would respond to a super-threshold excitation by an excursion in the phase space along the "ghosts" of the attractors destroyed in the homoclinic bifurcation ($J \leq 2.8J_{\mathrm{th}}$) and the boundary crisis ($2.8J_{\mathrm{th}} < J$), respectively, and would then return to the stable 2$^{\mathrm{nd}}$ ECM. Meaning that in contrast to the timeseries shown in Figs. 3(a) and 3(c) each super-threshold excitation is followed only by one pulse package. Subject to noise, the system can be excited if the perturbation introduced by the noise is large enough to overcome the excitability threshold. Figure 4(d) depicts t_{cor} (red triangles, right y-axis) and R_T (blue dots, left y-axis) as functions of the noise strength β for $K = 0.22921$ and $J = 2J_{\mathrm{th}}$, i.e., for a K-value closely above the homoclinic bifurcation at $K_{\mathrm{hom}} = 0.22920$. Furthermore, t_{cor} is shown for $K = 0.2314$ and $J = 3J_{\mathrm{th}}$ (black stars, right y-axis) as well as for $K = 0.24515$ and $J = 4J_{\mathrm{th}}$ (gray hexagons, right y-axis), i.e., for K-values closely above the crisis of the chaotic attractor at $K_{\mathrm{cris}}(J = 3J_{\mathrm{th}}) = 0.23324$ and $K_{\mathrm{cris}}(J = 4J_{\mathrm{th}}) = 0.24514$, respectively (cf. Fig. 2). A clear maximum of t_{cor} can be observed in all three cases indicating coherence resonance. Figures 4(a)–4(c) visualize the respective dynamics for values of β below ($\beta = 1 \cdot 10^{-10}$, Fig. 4(a)), at ($\beta_{\mathrm{opt}} = 5 \cdot 10^{-9}$, Fig. 4(b)), and above ($\beta = 6.5 \cdot 10^{-8}$, Fig. 4(c)) the noise strength β_{opt}, at which the maximum of t_{cor} is observed for $J = 2J_{\mathrm{th}}$. Analogously, Figs. 4(e)–4(g) depict time series below ($\beta = 0.02$, Fig. 4(e)), at ($\beta_{\mathrm{opt}} = 0.038$, Fig. 4(f)), and above ($\beta = 0.08$, Fig. 4(g)) the noise strengths $\beta_{\mathrm{opt}} = 0.23325$ of the coherence maximum for $J = 3J_{\mathrm{th}}$. The β-values, at which the time series are taken, are indicated by gray dashed vertical lines in Fig. 4(d).

Let us first discuss the coherence resonance close to the homoclinic bifurcation. Generally, the time between two excitations T_{ISI} can be decomposed into the time needed to activate the system t_a and the refractory time t_r, which the system needs to settle back to the rest state. In

#206726 - $15.00 USD Received 20 Feb 2014; revised 11 Apr 2014; accepted 6 May 2014; published 27 May 2014
(C) 2014 OSA

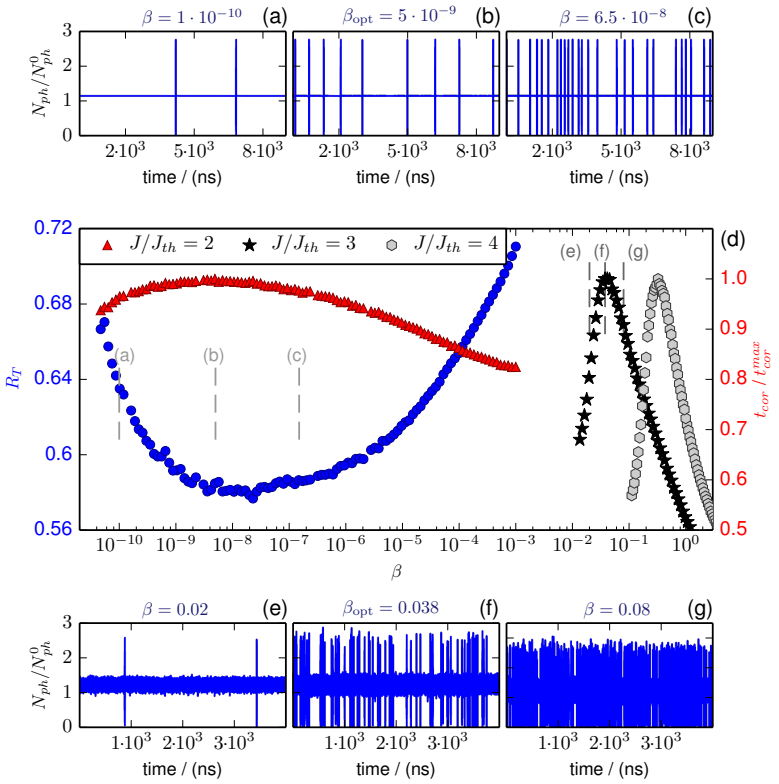

Figure 4. Stochastic dynamics: **(a)–(c)**: Time series for $J = 2J_{\text{th}}$ and $K = 0.2292$ for different β indicated by gray dashed lines in **(d)**. β_{opt} denotes the noise strength at the maximum of the coherence time. Central panel **(d)**: Normalized standard deviation of interspike interval R_T (blue dots) for $J = 2J_{\text{th}}$ and coherence time t_{cor} (normalized to its maximum value $t_{\text{cor}}^{\text{max}}$) versus noise strength β for $J = 2J_{\text{th}}$ (red triangles), $J = 3J_{\text{th}}$ (black stars), and $J = 4J_{\text{th}}$ (gray hexagons). In physical units the maximal coherence times are $\tau_{\text{ph}} t_{\text{cor}}^{\text{max}}(J = 2J_{\text{th}}) = 2.50\,\text{ns}$, $\tau_{\text{ph}} t_{\text{cor}}^{\text{max}}(J = 3J_{\text{th}}) = 2.39\,\text{ns}$, and $\tau_{\text{ph}} t_{\text{cor}}^{\text{max}}(J = 4J_{\text{th}}) = 1.93\,\text{ns}$. The feedback strength is $K = 0.22921$ for $J = 2J_{\text{th}}$, $K = 0.23325$ for $J = 3J_{\text{th}}$, and $K = 0.24515$ for $J = 4J_{\text{th}}$, respectively. **(e)–(g)**: Time series for $J = 3J_{\text{th}}$ and $K = 0.233325$ for different β indicated by gray dashed lines in **(d)**. Parameters as in Table 1.

#206726 - $15.00 USD Received 20 Feb 2014; revised 11 Apr 2014; accepted 6 May 2014; published 27 May 2014
(C) 2014 OSA

our system, the rest state is the stable 2nd ECM, and the refractory time is given by the time the system needs to spiral back to the 2nd ECM after one excitation. This means that t_r is fixed by the internal dynamics of the system, while t_a depends on the noise strength β. For low values of β, the activation time t_a is long compared to t_r (see Fig. 4(a)). Increasing β, it becomes easier for the system to overcome the excitation threshold and the pulse packages arise more regularly (see Fig. 4(b)). This is indicated by an increase of t_{cor} and a decrease of R_T. Increasing β further, pulse packages are excited more often, but the regularity of their appearance decreases and they are additionally deformed by the noise (see Fig. 4(c)). This leads to a decrease of t_{cor} and an increase of R_T. The maximum of t_{cor} does not coincide exactly with the minimum of R_T. This is expected, because t_{cor} accounts for coherence in periodicity of the pulse packages as well as coherence in amplitude fluctuations, while R_T only measures the periodicity of the pulse packages.

Higher pump currents of $J = 3J_{\mathrm{th}}$ and $J = 4J_{\mathrm{th}}$ lead to higher excitability thresholds (see Fig. 2(c)). Thus, a maximum of the correlation is therefore expected at a higher level of the noise. This is the reason why the maximum of t_{cor} shifts to higher values of the noise strength β with increasing J (see black stars and gray hexagons in Fig. 4(d) for $J = 3J_{\mathrm{th}}$ and $J = 4J_{\mathrm{th}}$, respectively). By comparing the time traces taken at the maxima of t_{cor} for $J = 2J_{\mathrm{th}}$ and $J = 3J_{\mathrm{th}}$, which are depicted in Figs. 4(b) and 4(f), respectively, two effects are prominent. On the one hand, the higher noise level in Fig. 4(f) becomes obvious, and, on the other hand, we see that the peak heights of the pulse package are varying more strongly in Fig. 4(f) than in Fig. 4(b), i.e., the amplitude jitter of the pulse packages is larger. However, the measure R_T fails at higher values of the noise strength, because there is an ambiguity in distinguishing the peak position from positions of extreme noise events. The trajectory is just distorted so much by the noise that the first dropout in ρ_{inv} crossing $\rho_{\mathrm{inv}}^{\mathrm{thr}}$ is not necessarily the beginning of a pulse package. Therefore, R_T has not been depicted for $J = 3J_{\mathrm{th}}$ and $J = 4J_{\mathrm{th}}$. That for $J = 3J_{\mathrm{th}}$ and $J = 4J_{\mathrm{th}}$ the dynamics beyond the coherence maximum is dominated by the noise can be seen in Fig. 4(g) depicting for $J = 3J_{\mathrm{th}}$ a time trace right to the maximum of t_{cor}.

In Fig. 5(a) the dependence of the feedback strengths K_{cris}, at which the boundary crisis occurs, is depicted as a function of the pump current. It reveals that K_{cris} increases linearly with the pump current J. As mentioned in Section 3, it was shown in previous works [7, 69] that the RO damping increases linearly with J. Further, the feedback strengths K_H of the first Hopf bifurcation marking the beginning of the first bifurcation cascade also reveals a linear dependence on J as discussed in [9, 51]. The linear dependence of K_{cris} on J shown in Fig 5(a) now suggest that the linear increase of K_{cris} with J is also due to the pump dependence of the RO damping. From Fig. 2(c), it can be presumed that this linear dependence of K_{cris} on J results in a square-root like increase of the projection of the excitability threshold onto the photon number $\Delta N_{\mathrm{ph}}^{\mathrm{thr}}$ with J. This can be seen as follows: $\Delta N_{\mathrm{ph}}^{\mathrm{thr}}$ is given by the difference of the photon number of the 2nd ECM (thick green lines in Fig. 2(c)) and its anti-mode (dashed black lines in Fig. 2(c)). The former increases square-root like with J, while the latter decreases with J in the same way, which causes the square-root like increase of $\Delta N_{\mathrm{ph}}^{\mathrm{thr}}$ depicted in Fig. 5(b). Since the increase of K_{cris} on J is relatively small in the current range plotted in Fig. 5(b), the increase of $\Delta N_{\mathrm{ph}}^{\mathrm{thr}}$ is nearly linear. Note that the threshold has always been determined at the same (very small) distance to K_{cris}, more precisely at $K = K_{\mathrm{cris}} + 1 \cdot 10^{-5}$. Eventually, the dependence of the noise strength at the coherence maximum β_{opt} on J is depicted in Fig. 5(c). The optimal noise level β_{opt} increases with J as expected from the increase of the threshold. To our knowledge, this is the first time coherence resonance has been observed close to a boundary crisis. Further, in contrast to coherence resonance close to a homoclinic bifurcation studied in [25, 32], the pump current dependence of the coherence maximum observed close to a crisis should facilitates the experimental accessibility of the excitable regime.

#206726 - $15.00 USD Received 20 Feb 2014; revised 11 Apr 2014; accepted 6 May 2014; published 27 May 2014
(C) 2014 OSA

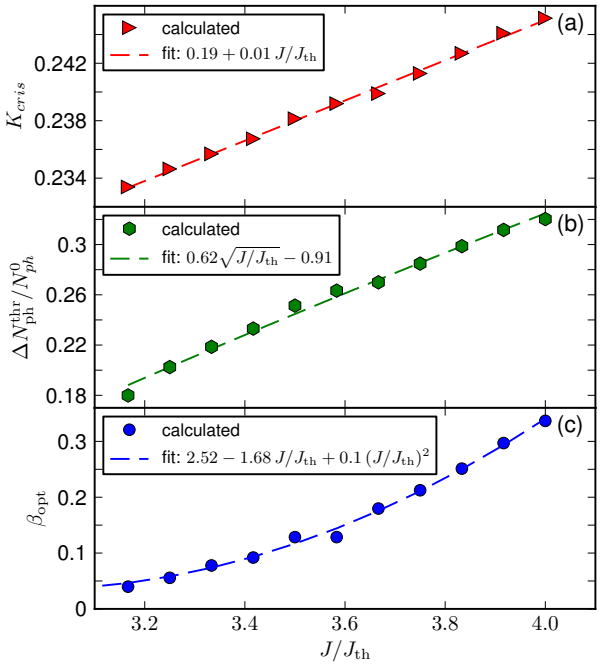

Figure 5. Dependence of **(a)**: the feedback strength $K_{\rm cris}$, at which the boundary crisis, occurs (red triangles), **(b)**: the photon number of the threshold $\Delta N_{\rm ph}^{\rm thr}$ (normalized to the photon number without feedback $N_{\rm ph}^{0}$) (green hexagones), and **(c)**: the optimal noise strength $\beta_{\rm opt}$ (blue circles) on pump current J (normalized to its threshold value $J_{\rm th}$). The dashed lines are best fits. Parameters as in Table 1.

In the remainder of this section, some practicalities of finding excitability and coherence resonance in laser systems are discussed. Experimentally it has been shown that spontaneous emissions noise is sufficient to excite a semiconductor laser under optical injection operating in a stable locked cw state close to the boundary of the locking tongue [17–19]. Further, excitability and coherence resonance has been experimentally observed in semiconductor lasers under optical feedback by adding broadband Gaussian white noise to the pump current [39,43]. Moreover, excitability close to a homoclinic bifurcation [25] and close to a crises [26] has been verified experimentally in an integrated multi-section semiconductor QW integrated feedback laser by perturbing the laser with short external optical pulses. Both methods, adding noise to the pump current and external optical pulses cause well tunable perturbations of the trajectory in the phase space. In our simulations, for simplicity we use the spontaneous emission noise in the field equation, i.e., the coefficient β, to excite the system. Since this is also a perturbation of the trajectory in the phase space, we expect that our results can be verified experimentally by the two methods mentioned above.

Further, our simulations have been performed for a fixed amplitude phase coupling α, a fixed band structure, and a fixed feedback phase C, but they are robust under changes of these parameters as discussed in the following. From the transcendental Eq. (6), it can be seen that the number of ECMs and thus the number of bifurcation cascades increases with τ and α (See [61] for a detailed discussion.). We have focused on the simplest scenario, of a short external cavity and a small α-factor, where only one instability region is observed. However, excitable regimes and crises can also be found for larger values of α and τ for which several bifurcation

#206726 - $15.00 USD Received 20 Feb 2014; revised 11 Apr 2014; accepted 6 May 2014; published 27 May 2014
(C) 2014 OSA

cascades occur [50,70]. The band structure mainly impacts on the damping of the ROs, which in terms influences the dynamical stability of the laser. For experimental realizations the enhanced dynamical stability of QD lasers is a big advantage, because the structure of the bifurcation cascade is simpler [50, 71], and they are thus less sensitive to perturbations unavoidable in experiments, e.g., small temperature fluctuations. Therefore, we expect that with a QD lasers it should be easier to detect the excitable regime and stay close to a homoclinic bifurcation or a boundary crises. Eventually, our results are robust under changes of the feedback phase C, that mainly shifts the range of K values at which the bifurcations occur. As mentioned above excitability has been demonstrated in multi-section integrated feedback laser, which reveals that the feedback parameters, especially the phase C and the feedback strength K, can be controlled well enough to stay close to the homoclinic bifurcation or the crises of the chaotic attractor. Indeed it has been shown that the bifurcation cascade can be scanned by careful tuning of external cavity phase C and pump current [72, 73].

5. Conclusion

We found that a QD laser subject to optical feedback can be operated in an excitable regime, where the regularity of the emitted spikes is sensitive to the noise strength as well as to the pump current. More precisely, we have shown that coherence resonance exists close to a boundary crisis of a chaotic attractor. In contrast to coherence resonance close to a homoclinic bifurcation, which was theoretically predicted previously, this type of coherence resonance has the advantage to be highly sensitive to variations of the pump current. This permits to shift the excitability threshold and, consequently, the maximum of the coherence found in the emitted spikes. Further, our findings are robust over a large range of pump currents facilitating the experimental accessibility of the excitable regime. Since the operating pump current is easily accessible in an experiment, it opens up the possibility to experimentally observe coherence resonance in semiconductor QD lasers. Further, we connect the pump current induced shift of the boundary crisis to the damping of the turn-on relaxations, as it also increases linearly with the pump strength.

A. Derivation of the dimensionless model

In this section, the dimensionless version of the dynamical equations (1) used in the main text is derived from the physical model. The optical subsystem of the QD laser model with feedback is described by a Lang-Kobayashy type delay differential equation for the normalized slowly varying complex amplitude $\mathscr{E}(t)$ of the electric field $E(t) = \frac{1}{2}\left(\mathscr{E}(t)e^{i2\pi\nu_{\mathrm{th}}t} + \mathrm{c.c}\right)$, where ν_{th} is the optical frequency at lasing threshold, and c. c denotes the complex conjugate. Since different dynamics is taken into account for electrons and holes the carrier subsystem consists of four coupled differential equations for the occupation probabilities ρ_e and ρ_h of electrons and holes in the discrete QD ground states, and the carrier densities for electrons, w_e, and holes, w_h, in the surrounding QW acting as a carrier reservoir

$$\frac{d\mathscr{E}}{dt} = \frac{1+i\alpha}{2}\left[2\bar{W}Z_a^{\mathrm{QD}}(\rho_e+\rho_h-1)-\tau_{\mathrm{ph}}^{-1}\right]\mathscr{E} + \frac{K}{\tau_{\mathrm{in}}}e^{-iC}\mathscr{E}(t-t_{\mathrm{ec}}) + \sqrt{\beta Z_a^{\mathrm{QD}}W\rho_e\rho_h}\xi, \quad (11a)$$

$$\frac{d\rho_e}{dt} = S_e^{\mathrm{in}}(1-\rho_e) - S_e^{\mathrm{out}}\rho_e - \bar{W}(\rho_e+\rho_h-1)N_{\mathrm{ph}} - W\rho_e\rho_h, \quad (11b)$$

$$\frac{d\rho_h}{dt} = S_h^{\mathrm{in}}(1-\rho_h) - S_h^{\mathrm{out}}\rho_h - \bar{W}(\rho_e+\rho_h-1)N_{\mathrm{ph}} - W\rho_e\rho_h, \quad (11c)$$

$$\frac{dw_e}{dt} = \frac{j}{e_0} - 2N^{\mathrm{QD}}\left[S_e^{\mathrm{in}}(1-\rho_e) - S_e^{\mathrm{out}}\rho_e\right] - B^S w_e w_h, \quad (11d)$$

$$\frac{dw_h}{dt} = \frac{j}{e_0} - 2N^{\mathrm{QD}}\left[S_h^{\mathrm{in}}(1-\rho_h) - S_h^{\mathrm{out}}\rho_h\right] - B^S w_e w_h. \quad (11e)$$

#206726 - $15.00 USD Received 20 Feb 2014; revised 11 Apr 2014; accepted 6 May 2014; published 27 May 2014
(C) 2014 OSA

Here, the phase amplitude coupling is described by the linewidth enhancement factor α. Further, the optical intensity losses for the laser device of length L are given by the inverse of the photon lifetime $\tau_{\rm ph}$. They are balanced by the linear gain term $2\bar{W}Z_a^{\rm QD}(\rho_e+\rho_h-1)$, where $\bar{W}Z_a^{\rm QD}$ is the linear gain coefficient for the processes of induced emission and absorption. The gain coefficient is proportional first to the Einstein coefficient of induced emission $\bar{W}$ that measures the coherent interaction between the two-level system and the laser mode, and second to the number $Z_a^{\rm QD}$ of lasing QDs inside the waveguide (the factor 2 is due to spin degeneracy). The number of lasing QDs, $Z_a^{\rm QD}$, is given by $Z_a^{\rm QD}\equiv a_L A N_a^{\rm QD}$, where a_L is the number of self-organized QD layers, A is the in-plane area of the QW, and $N_a^{\rm QD}$ is the density per unit area of the active QDs. As a result of the size distribution and of the material composition fluctuations of the QDs, the gain spectrum is inhomogeneously broadened, and only a subgroup (density $N_a^{\rm QD}$) of all QDs ($N^{\rm QD}$) matches the mode energies for lasing. Taking into account only one roundtrip of the light in the external cavity, the field amplitude $\mathscr{E}(t-\tau_{\rm ec})$ delayed by the external cavity roundtrip time $\tau_{\rm ec}$ is coupled back into the laser with feedback strength K and rotated by the external cavity phase $C\equiv 2\pi\nu_{\rm th}\tau_{\rm ec}$. The roundtrip time of the light in the laser of length L is denoted by $\tau_{\rm in}\equiv 2L\sqrt{\varepsilon_{\rm bg}}/\tilde{c}$ with the background permittivity $\varepsilon_{\rm bg}$, and the speed of light $\tilde{c}$. Although being completely determined by $\nu_{\rm th}$ and $\tau_{\rm ec}$, the feedback phase C is usually treated as an independent parameter since small variations of the external cavity length cause a variation of the phase C over its full range $[0,2\pi]$, while the external roundtrip time $\tau_{\rm ec}$ is hardly affected by these fluctuations [65, 74, 75].

The spontaneous emission is modeled by bimolecular recombination $\beta Z_a^{\rm QD} W\rho_e\rho_h$, where β is the spontaneous emission factor measuring the probability that a spontaneously emitted photon is emitted into the lasing mode. The Einstein coefficient for spontaneous emission is denoted by W. It can be determined by calculating the coherent interaction of a two-level system, i.e., a single QD, with all resonator modes in the framework of the second quantization [58]. Note that the coefficients $\bar{W}$ and W differ by three orders of magnitude (See Refs. [8,60] for details of their derivation.). In a semiclassical approach, the process of spontaneous emission is modeled by a complex Gaussian white noise term $\xi=\xi(t)$, i.e.,

$$\begin{aligned}\xi(t)&=\xi_a(t)+i\xi_b(t),\quad \langle\xi_i(t)\rangle=0,\\ \langle\xi_a(t)\xi_b(\tilde{t})\rangle&=\delta_{a,b}\delta(t-\tilde{t}),\quad \text{for}\quad \xi_i(t)\in\mathbb{R}, i\in\{a,b\}.\end{aligned}$$

Here, subscripts a and b stand for real and imaginary parts, respectively.

In the model, the carrier exchange between QW and QDs is mediated by non-constant microscopically calculated Coulomb in- ($S_{e/h}^{\rm in}$) and out-scattering ($S_{e/h}^{\rm out}$) rates [54, 56], which are nonlinear functions of the carrier densities of electrons (w_e) and holes (w_h) in the carrier reservoir, and therefore depend on the pump current density j. The latter is normalized by the elementary charge e_0 in the equations for the reservoir densities (Eqs. (11d) and (11e)). The inverse of the sum of the scattering rates yields the carrier lifetimes $\tau_{e/h}\equiv(S_{e/h}^{\rm in}+S_{e/h}^{\rm out})^{-1}$ in the QD levels. Note that in thermodynamic equilibrium, there is a detailed balance between in- and out-scattering rates, which allows one to relate the coefficients of in- and out-scattering even away from the thermodynamic equilibrium [76]. The detailed balance relation for in- and out-scattering rates for the quasi-equilibrium then reads [59]

$$S_{e/h}^{\rm out}(w_e,w_h)=S_{e/h}^{\rm in}(w_e,w_h)e^{-\frac{\Delta E_{e/h}}{k_{\rm bo}\mathscr{T}}}\left[e^{\frac{w_{e/h}}{D_{e/h}k_{\rm bo}\mathscr{T}}}-1\right]^{-1}. \tag{12}$$

It shows that the scattering rates strongly depend on the energy differences $\Delta E_e\equiv E_e^{\rm QW}-E_e^{\rm QD}$ and $\Delta E_h\equiv E_h^{\rm QD}-E_h^{\rm QW}$ between the QD levels, E_e^{QD} and $E_h^{\rm QD}$, and the band edges of the QW,

#206726 - $15.00 USD Received 20 Feb 2014; revised 11 Apr 2014; accepted 6 May 2014; published 27 May 2014
(C) 2014 OSA

E_e^{QW} and E_h^{QW}, for electrons (e) and holes (h), respectively. The carrier degeneracy concentrations are given by $D_{e/h} k_{\mathrm{bo}} \mathscr{T}$, where $D_{e/h} \equiv m_{e/h}/(\pi\hbar^2)$ are the 2D densities of state in the carrier reservoir with the effective masses $m_{e/h}$. The temperature is denoted by $\mathscr{T}$ and k_{bo} is Boltzmann's constant (see [60] for fit functions for the in-scattering rates $S_{e/h}^{\mathrm{in}}$). Analogously to the spontaneous emission in the field equations, the spontaneous emission in the QW is incorporated by the bimolecular term $B^S w_e w_h$, where B^S is the band-band recombination coefficient (see Eqs. (11d) and (11e)). All physical parameters used are summarized in Table 2.

Table 2. Physical parameters used in the simulation of the QD laser model unless stated otherwise.

symbol	value	symbol	value	symbol	value
W	$0.7\,\mathrm{ns}^{-1}$	A	$4\cdot10^{-5}\,\mathrm{cm}^2$	$\mathscr{T}$	$300K$
$\bar{W}$	$0.11\,\mu\mathrm{s}^{-1}$	N_a^{QD}	$0.3\cdot10^{10}\,\mathrm{cm}^{-2}$	L	$1\,\mathrm{mm}$
τ_{ph}^{-1}	$0.1\,\mathrm{ps}^{-1}$	N^{QD}	$1\cdot10^{11}\,\mathrm{cm}^{-2}$	ε_{bg}	14.2
β	$2.2\cdot10^{-3}$	B^S	$540\,\mathrm{ns}^{-1}\,\mathrm{nm}^2$	τ_{in}	$24\,\mathrm{ps}$
a_L	15	Z_a^{QD}	$1.8\cdot10^6$	m_e	$0.043\,m_0$
λ_{opt}	$1.3\,\mu\mathrm{m}$	ν_{th}	230 THz	m_h	$0.45\,m_0$
ΔE_e	210 meV	ΔE_h	50 meV	j_{th}	$6.72\cdot10^5\,\frac{\mathrm{A}}{\mathrm{m}^2}$
τ_{ec}	160 ms	C	π	K	$[0,1]$

In the main text, a dimensionless form of the dynamical equations is used, which emphasizes the different timescales involved. As it is usually done for rate equation models of semiconductor lasers, time is rescaled with respect to the photon lifetime τ_{ph} [77]. Introducing the dimensionless time $t' \equiv t/\tau_{\mathrm{ph}}$ as well as the dimensionless reservoir populations $W_e \equiv w_e/(2N^{\mathrm{QD}})$ and $W_h \equiv w_h/(2N^{\mathrm{QD}})$, the set of dimensionless dynamical equations (1) discussed in the main text can be derived. Where the dimensionless linear gain coefficient g, the rescaled feedback strength k, the dimensionless delay time τ, the dimensionless coefficient of the spontaneous emission r_{sp}, the ratio of photon and carrier lifetimes γ (Here the lifetime of the carrier subsystem is represented by W^{-1}.), the ratio of the Einstein-factors of induced and spontaneous emission r_w, the dimensionless pump rate J, the coefficient of spontaneous and non-radiative losses in the carrier reservoir c, and the dimensionless scattering rates $s_{e/h}^{\mathrm{in/out}}$ have been introduced as

$$g \equiv 2a_L \bar{W} A N_a^{\mathrm{QD}} \tau_{\mathrm{ph}}, \quad k = K\frac{\tau_{\mathrm{ph}}}{\tau_{\mathrm{in}}}, \qquad \tau = \frac{\tau_{\mathrm{ec}}}{\tau_{\mathrm{ph}}}, \qquad r_{\mathrm{sp}} \equiv W Z_a^{\mathrm{QD}} \tau_{\mathrm{ph}}, \quad \gamma \equiv \tau_{\mathrm{ph}} W,$$

$$r_w \equiv \frac{\bar{W}}{W}, \qquad J \equiv \frac{j}{2N^{\mathrm{QD}} e_0 W}, \quad c \equiv \frac{B^S 2N^{\mathrm{QD}}}{W}, \quad \text{and} \quad s_{e/h}^{\mathrm{in/out}} \equiv \frac{1}{W} S_{e/h}^{\mathrm{in/out}}.$$

The values of the dimensionless parameters corresponding to the physical parameters of Table 2, are listed in Table 1. Note, that the small parameter γ multiplying the right hand sides of Eqs. (1b)–(1e) expresses the timescale separation between the fast field equation and the slow subsystem of the carriers, i.e., the QD laser is a slow-fast system if the scattering rates $s_{e/h}^{\mathrm{in/out}}$ are not to large.

#206726 - $15.00 USD Received 20 Feb 2014; revised 11 Apr 2014; accepted 6 May 2014; published 27 May 2014
(C) 2014 OSA

Acknowledgments

We thank R. Aust and A. Zakharova for fruitful discussions. This work was supported by DFG in the framework of SFB 910 and SFB 787.

#206726 - $15.00 USD Received 20 Feb 2014; revised 11 Apr 2014; accepted 6 May 2014; published 27 May 2014
(C) 2014 OSA